

Polarity Loss for Zero-shot Object Detection

Shafin Rahman^{*†}, Salman Khan^{†‡*} and Nick Barnes^{†*}

^{*}Australian National University, [†]Data61-CSIRO, [‡]Inception Institute of AI

firstname.lastname@anu.edu.au

Abstract

Zero-shot object detection is an emerging research topic that aims to recognize and localize previously ‘unseen’ objects. This setting gives rise to several unique challenges, e.g., highly imbalanced positive vs. negative instance ratio, ambiguity between background and unseen classes and the proper alignment between visual and semantic concepts. Here, we propose an end-to-end deep learning framework underpinned by a novel loss function that puts more emphasis on difficult examples to avoid class imbalance. We call our objective the ‘Polarity loss’ because it explicitly maximizes the gap between positive and negative predictions. Such a margin maximizing formulation is important as it improves the visual-semantic alignment while resolving the ambiguity between background and unseen. Our approach is inspired by the embodiment theories in cognitive science, that claim human semantic understanding to be grounded in past experiences (seen objects), related linguistic concepts (word dictionary) and the perception of the physical world (visual imagery). To this end, we learn to attend to a dictionary of related semantic concepts that eventually refines the noisy semantic embeddings and helps establish a better synergy between visual and semantic domains. Our extensive results on MS-COCO and Pascal VOC datasets show as high as $14\times$ mAP improvement over state of the art.¹

1. Introduction

Zero shot learning (ZSL) is considered the ‘holy-grail’ among transfer learning problems. The goal is to reason about objects that have never been seen before. Traditional ZSL literature only focuses on ‘recognizing’ unseen objects. Since real-world objects only appear as a part of a complete scene, the newly introduced zero shot object detection (ZSD) task [36] considers a more practical setting where the goal is to simultaneously ‘locate and recognize’ unseen objects. A successful ZSD system can help pave the way for lifelong learning machines that intelligently discover new objects and incrementally enhance their knowledge.

Recently, the initial attempts on ZSD have been reported

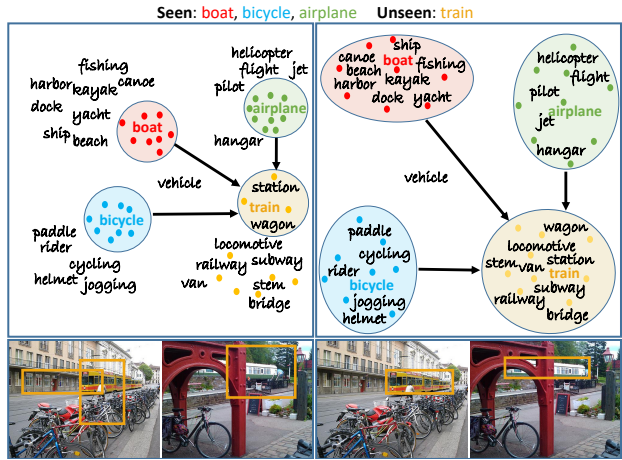


Figure 1: (Top Left) Traditional ZSD approaches align visual features (solid dots) to their corresponding semantics (boat/airplane/bicycle) without considering the related semantic concepts (black text). It results in a fragile description of an unseen class (train) and causes confusion with background and seen classes (bottom left). (Top Right) Our approach automatically attends to related semantics from an external vocabulary and reshapes the semantic embedding such that visual features are well-aligned with seen word vectors and related semantics. Moreover, it maximizes the inter-class separation that avoids confusion between unseen and background (bottom right).

[5, 8, 36, 51]. We note that these efforts suffer from serious limitations, e.g, (a) lack of an end-to-end trainable pipeline [5], (b) confusion between background and unseen classes [5, 51], (c) inability to update semantic embeddings based on relationships between visual and semantic concepts [5, 8], (d) bounding box prediction does not directly benefit from the semantic information [5, 8, 36, 51], (e) inability to predict bounding boxes specific to unseen objects [36, 5], (f) dependence on pre-trained weights that were learned on datasets containing unseen objects [5, 8].

In this work, we propose an integrated deep learning framework for ZSD that addresses the above-mentioned challenges. Our framework is motivated by embodiment theories in cognitive science that explain how the brain understands and processes semantic information. Dual coding theory [32] hypothesizes that concrete concepts (‘nouns’)

¹Code and evaluation protocols available at: TBA.

are represented by the human brain as a combination of linguistic and visual codes. Recent fMRI and computational modeling studies [3, 4] confirm that a word’s meaning is encoded within the brain as a distribution over related semantics (e.g., a vocabulary) as well as grounded in sensorimotor experience (e.g., visual perception). Consequently, our approach leverages three information sources to reason about unseen categories (see Fig. 1): (a) the seen objects and their relationship with the unseen, (b) visually grounded semantic concepts in images and (c) an external linguistic vocabulary.

The core of our approach is a novel loss function that builds upon Focal loss [26] for generic object detection. While Focal loss only promotes correct prediction, we observe that a successful ZSL system should also learn to minimize projections on representative vectors for negative classes. Our proposed loss jointly maximizes projection on correct classes and minimizes the alignment with incorrect ones. This approach effectively allows distinction between background *vs.* unseen classes and promotes better alignment between visual and semantic concepts. Our main contributions are:

- A novel loss function called ‘*Polarity loss*’ to address imbalance and achieve maximal separation between positive and negative tag predictions.
- An end-to-end ZSD framework that learns to relate an external vocabulary of words, class embeddings and visual information. This approach helps to reshape the word embeddings based on visual-semantic relations.
- A new seen-unseen split on MS-COCO dataset that respects practical considerations such as diversity and rarity among unseen classes.
- Extensive experiments on old and new MS-COCO dataset splits and Pascal VOC datasets which give absolute gains of 9.3 and 7.6 in mAP over [5] and [8] respectively. This amounts to a massive $14\times$ improvement over [5] on challenging MS-COCO dataset.

2. Related work

Object detection: End-to-end trainable deep learning models have set new performance records on object detection benchmarks. The most popular deep architectures can be categorized into double stage networks (e.g., Faster-RCNN [38], RFCN [16]) and single stage networks (e.g., SSD[29], YOLO[37]). Generally, double-stage detectors achieve high accuracy, while single-stage detectors work faster. To further improve the performance, recent object detectors introduce novel concepts such as feature pyramid network (FPN) [27, 20] instead of region proposal network (RPN), focal loss [26] instead of traditional cross-entropy loss, non-rectangular region selection [46] instead of rectangular bounding box, designing backbone architecture [24] instead of ImageNet pre-trained networks (e.g.,

VGG[41]/ResNet[13]). In this paper, we attempt to extend object detection to the next level: detecting unseen objects which are not observed during training.

Zero-shot learning: The ZSL literature is predominated by classification approaches that focus on single [12, 45, 21, 35, 49, 19] or multi-label [22, 34] recognition. The extension of conventional ZSL approaches to zero-shot object localization/detection is relatively less investigated. Among previous attempts, Li *et al.* [23] learned to segment attribute locations which can locate unseen classes. [15] used a shared shape space to segment novel objects that look like seen objects. These approaches are useful for classification but not extendable to ZSD. [14, 25] proposed novel object localization based on natural language description. Few other methods located unseen objects with weak image-level labels [34, 39]. However, none of them perform ZSD. Very recently, [36, 51, 5, 8] investigated the ZSD problem. These methods can detect unseen objects using box annotations of seen objects. Among them, [5] proposed a feature based approach where object proposals are generated by edge-box [52], and [36, 51, 8] modified the object detection frameworks [38, 37] to adapt ZSD settings. The generalization of this problem is called generalized-ZSD (GZSD) which aims to detect both seen and unseen objects together [5]. Here, we propose a new loss formulation that can greatly benefit single stage zero-shot object detectors.

3. Max-margin cross-entropy

3.1. Balanced Cross-Entropy vs. Focal loss

Consider a binary classification task where $y \in \{0, 1\}$ denotes the ground-truth class and $p \in [0, 1]$ is the prediction probability for the positive class (i.e., $y = 1$). The standard binary cross-entropy (CE) formulation gives:

$$\text{CE}(p, y) = -\alpha_t \log p_t, \quad p_t = \begin{cases} p, & \text{if } y = 1 \\ 1 - p, & \text{otherwise.} \end{cases} \quad (1)$$

where, α is a loss hyper-parameter representing inverse class frequency and the definition of α_t is analogous to p_t . In the object detection case, the object *vs.* background ratio is significantly high (e.g., 10^{-3}). Using a weight factor α is a traditional way to address this strong imbalance. However, being independent of the model’s prediction, this approach treats both well-classified (easy) and poorly-classified (hard) cases equally. It favors easily classified examples to dominate the gradient and fails to differentiate between easy and hard examples. To address this problem, Lin *et al.* [26] proposed ‘Focal loss’ (FL):

$$\text{FL}(p, y) = -\alpha_t (1 - p_t)^\gamma \log p_t \quad (2)$$

where, $\gamma \in [0, 5]$ is a loss hyper-parameter that dictates the slope of cross entropy loss (a large value denotes higher

slope). The term $(1 - p_t)^\gamma$ enforces a high and low penalty for hard and easy examples respectively. In this way, FL simultaneously addresses object vs. background imbalance and easy vs. hard examples difference during training.

Shortcomings: In zero-shot learning, it is highly important to align visual features with semantic word vectors. This alignment requires the training procedure to (1) push visual features close to their ground-truth embedding vector and (2) push them away from all negative class vectors. FL can only perform (1) but cannot enforce (2) during the training of ZSD. Therefore, although FL is well-suited for traditional seen object detection, but not for the ZSD scenario.

3.2. Polarity Loss definition

To address the above-mentioned shortcomings, we propose a margin maximizing loss formulation that is particularly suitable for ZSD. This formulation is generalizable and can work with loss functions other than Eqs. 1 and 2. However, for the sake of comparison with the best model, we base our analysis on the state of the art FL.

Multi-class Loss: Consider that a given training set $\{\mathbf{x}, \mathbf{y}\}_i$ contains N examples belonging to C object classes plus an additional background class. For the multi-label prediction case, the problem is treated as a sum of individual binary cross-entropy losses where each output neuron decides whether a sample belongs to a particular object class or not. Assume, $\mathbf{y} = \{y^i \in \{0, 1\}\} \in \mathbb{R}^C$ and $\mathbf{p} = \{p^i \in [0, 1]\} \in \mathbb{R}^C$ denote the ground-truth label and prediction vectors respectively, and the background class is denoted by $\mathbf{y} = \mathbf{0} \in \mathbb{R}^C$. Then, the FL for a single box proposal is:

$$\mathcal{L} = \sum_i -\alpha_t^i (1 - p_t^i)^\gamma \log p_t^i. \quad (3)$$

Polarity Loss: Suppose, for a given bounding box feature containing an ℓ^{th} object class, p^ℓ represents the prediction value for the ground-truth object class, *i.e.*, $y^\ell = 1$, see Table 1. Note that $p^\ell = 0$ for the background class (where $y^i = 0 \forall i$). Ideally, we would like to maximize the predictions for ground-truth classes and simultaneously minimize prediction scores for all other classes. We propose to explicitly maximize the margin between predictions for positive and negative classes to improve the visual-semantic alignment for ZSD. This leads to a new loss function that we term as ‘Polarity Loss’ (PL), represented by:

$$\mathcal{L}_{PL} = \sum_i f_p(p^i - p^\ell) \text{FL}(p^i, y^i), \quad (4)$$

where, f_p is a monotonic penalty function. For any prediction, p^i where $\ell \neq i$, the difference $p^i - p^\ell$ represents the disparity between the true class prediction and the prediction for the negative class. The loss function enforces a large negative margin to push prediction values p^i and p^ℓ further

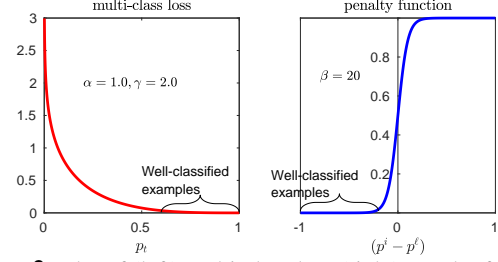


Figure 2: Plot of (left) multi-class loss (right) penalty function.

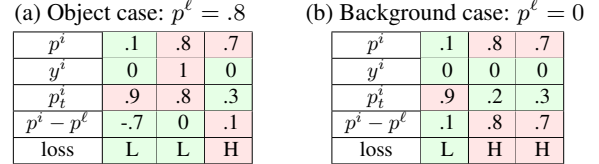


Table 1: A toy example. Intermediate computations for Polarity Loss are shown. Low (L) values are shown in green while High (H) values are shown in red. A mismatch between $(p^i$ and $y^i)$ + a close match between $(y^i$ and $y^\ell)$ results in a high loss.

part. Therefore, for an object anchor case, the above objective enforces $p^\ell > p^i$, while for background case $0 > p^i$ *i.e.*, all p^i ’s are pushed towards zero (since $p^\ell = 0$).

Our Penalty Function: The f_p should necessarily be a ‘monotonically increasing’ function. It offers a small penalty if gap $p^i - p^\ell$ is low and a large penalty if the gap is high. This constraint enforces that $p^i < p^\ell$. In this paper, we implement f_p with β parameterized sigmoid function:

$$f_p(p^i - p^\ell) = \frac{1}{1 + \exp(-\beta(p^i - p^\ell))} \quad (5)$$

For the case when $p^i = p^\ell$, FL part guides the loss because f_p becomes a constant. We choose a sigmoid form for f_p because the difference $(p^i - p^\ell) \in [-1, 1]$ and f_p can be bounded by $[0, 1]$, similar to α_t or $(1 - p_t)$ factor of FL. Note that, it is not compulsory to stick with this particular choice of f_p . We also test a softplus based function for f_p in the supplementary material which is equally applicable.

Final Objective: The final form of the loss is:

$$\mathcal{L}_{PL}(\mathbf{p}, \mathbf{y}) = \sum_i \frac{-\alpha_t^i (1 - p_t^i)^\gamma \log p_t^i}{1 + \exp(-\beta(p^i - p^\ell))}, \text{ where,}$$

$$p_t^i = \begin{cases} p^i, & \text{if } y^i = 1 \\ 1 - p^i, & \text{otherwise} \end{cases} \quad p^\ell = p^i \llbracket y^i = 1 \rrbracket, \quad (6)$$

where, $\llbracket \cdot \rrbracket$ denotes the Iverson bracket.

A Toy Example: We explain the proposed loss with a toy example in Table 1 and Fig. 2. When an anchor box belongs to an ‘object’ and $p_t^i \geq .5$ (high) then $p^i - p^\ell \leq 0$ (low). From Fig. 2, both a multi-class loss and the penalty

function `find_low_loss` which eventually calculates a low loss. Similarly, when $p_t^i < .5$ (low), $p^i - p^\ell > 0$ (high), which evaluates to a high loss. When an anchor belongs to ‘background’, $p^i - p^\ell \geq 0$ and a high p^i results in a high value for both multi-class loss and the penalty function and vice versa. In this way, the penalty function always supports multi-class loss based on the disparity between the current prediction and ground-truth class’s prediction.

Polarity Loss Properties: The PL has two intriguing properties: (a) *Word-vectors alignment*: For ZSL, generally visual features are projected onto the word-vectors in semantic space. A high projection score indicates proper alignment with a word-vector. The overall goal of training is to achieve good alignment between the visual feature and its corresponding word-vector and an inverse alignment with all other word-vectors. In our proposed loss, $FL(\cdot)$ and f_p perform the direct and inverse alignment respectively. (b) *Class imbalance*: The penalty function f_p follows a trend similar to α_t and $(1-p_t)^\gamma$. It means that f_p assigns a low penalty to well-classified/easy examples and a high penalty to poorly-performed/hard cases. It greatly helps in tackling class imbalance for single stage detectors where negative boxes heavily outnumber positive detections.

4. Vocabulary metric

Apart from proper visual-semantic alignment and class imbalance, a significant challenge for ZSD is the inherent noise in the semantic space. In this paper, we propose a new ‘vocabulary metric learning’ approach to improve the quality of word vectors for ZSL tasks. For brevity of expression, we restrict our discussion to the case of classification probability prediction or bounding box regression for a single anchor. Suppose, the visual feature of that anchor, \mathbf{a} is $\phi(\mathbf{a}) = \mathbf{f}$, where ϕ represents the detector network. The total number of seen classes is S and a matrix $W_s \in \mathbb{R}^{S \times d}$ denotes all the d -dimensional word vectors of S seen classes arranged row-wise. The detector network ϕ is augmented with FC layers towards the head to transform the visual feature \mathbf{f} to have the same dimension of word vectors, i.e., $\mathbf{f} \in \mathbb{R}^d$. In Fig. 3, we describe several ways to learn the alignment function between visual features and semantic information. We elaborate them further below.

4.1. Learning with Word-vectors

For the traditional detection case shown in Fig. 3(a), the visual features \mathbf{f} are transformed with a learnable FC layer $W_d \in \mathbb{R}^{S \times d}$, followed by a sigmoid/softmax activation (σ) to calculate S prediction probabilities, $\mathbf{p}_d = \sigma(W_d \mathbf{f})$. This approach works fine for traditional object detection, but it is not suitable for the zero-shot settings as the transformation W_d cannot work with unseen object classes.

A simple extension of the traditional detection framework to the zero-shot setting is possible by replacing train-

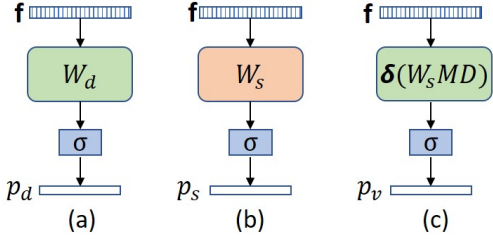


Figure 3: (a) Traditional basic approach with learnable W_d , (b) Inserting word vectors as a fixed embedding W_s , (c) learnable word vectors with vocabulary metric $\delta(W_s MD)$.

able weights of the FC layers, W_d by the non-trainable seen word vectors W_s (Fig. 3(b)). Keeping this layer frozen, we allow projecting the visual feature \mathbf{f} to the word embedding space to calculate prediction scores \mathbf{p}_s :

$$\mathbf{p}_s = \sigma(W_s \mathbf{f}) \quad (7)$$

This projection aligns visual features with the word vector of the corresponding true class. The intuition is that rather than directly learning a prediction score from visual features (in Fig 3(a)), it is better to learn a correspondence between the visual features with word vectors before the prediction.

Challenges with Basic Approach: Although the configuration described in Fig. 3(b) delivers a basic solution to zero-shot detection, it suffers from several limitations. (1) *Fixed Representations*: With a fixed embedding W_s , the network cannot update the semantic representations and has limited flexibility to properly align visual and semantic domains. (2) *Limited word embeddings*: The word embedding space is usually learned with billions of words from unannotated texts which results in noisy word embeddings. Understanding the semantic space with only S word vectors is therefore unstable and insufficient to model visual-semantic relationships. (3) *Unseen-background confusion*: In ZSD, one common problem is that the model confuses unseen objects with background since it has not seen any visual instances of unseen classes [51, 5].

4.2. Learning with vocabulary metric

To solve the above gaps, we propose to learn a more expressive and flexible semantic domain representation. Such representation can lead to a better alignment between visual features and word vectors. Precisely, we propose a vocabulary metric method summarized in Fig. 3(c) that takes advantage of the word vectors of a pre-defined vocabulary, $D \in \mathbb{R}^{v \times d}$ (where v is the number of words in the vocabulary) to better understand the word embedding space and has an inherent mechanism to update it accordingly for ZSD. Now, we calculate the prediction score as follows:

$$\mathbf{p}_v = \sigma(\delta(W_s MD) \mathbf{f}) \quad (8)$$

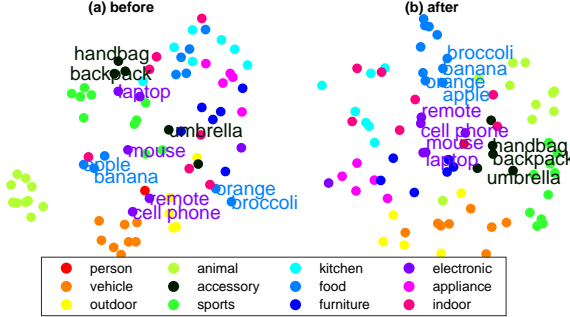


Figure 4: 2D tSNE [43] embedding of word2vec: (a) before (b) after modification based on vocabulary metric with our loss. Word-vectors are more evenly distributed in (b) than (a). Also, visually similar classes for example, apple/banana/orange/broccoli, cell phone/remote/laptop/mouse and handbag/backpack/umbrella are embedded more closely in (b) than (a). Super-category annotations are used for visualization only, not during our training.

Here, $M \in \mathbb{R}^{d \times v}$ represents the learnable parameters which connect seen word vectors with the vocabulary word vectors and $\delta(\cdot)$ is a tanh activation function. M can be interpreted as learned attention over the dictionary. It helps the network to update the word embedding space for better alignment with visual features. Simultaneously, the network can understand the semantic space better and learn a rich representation because it considers more linguistic examples (vocabulary words) inside the semantic space. Further, it helps to reduce unseen-background confusion since the network can relate visual features more accurately with a diverse set of linguistic concepts. We visualize word vectors before and after the update in Fig. 4 (a) and (b) respectively.

Here, we find it important to emphasize that the previous attempts to use such an external vocabulary have their respective limitations. For example, [2] considered a limited set of attribute while [1] used several disjoint training stages. These approaches are therefore not end-to-end trainable. Further, they only investigate the recognition problem.

Regression branch with semantic: Eq. 8 allows predicting seen class probabilities at the classification branch with the help of semantic information from vocabulary metric. Similarly, we can apply such semantic information in the regression branch with some additional trainable FC layers. In our experiment, we find that adding semantic information helps to improve the ZSD performance. It shows that the predicted regression box can benefit from the semantic information that improves the overall performance.

5. The single-stage detector

Our proposed ZSD framework is specially designed to work with single-stage detectors. The primary motivation is the direct connection between anchor classification and localization that ensures a strong feedback for both tasks. For

this study, we choose a recent unified single architecture, RetinaNet [26] to implement our proposed method. RetinaNet is the best detector known for its high speed (on par with single-stage detectors) and top accuracy (outperforming two-stage detectors). In Fig. 5, we illustrate the overall architecture of the model. In addition to a novel loss formulation, we also perform modifications to the RetinaNet architecture to link visual features (from ResNet50 [13]) with semantic information. Similar to [26], each pyramid level is connected to a classification and box regression subnet which shares its parameters across all pyramid levels. To adapt this network to ZSL setting, we perform simple modifications in both subnets to consider word-vectors (with vocabulary metric) during training (see Fig. 5). More architecture details are provided in the supplementary material.

Training: We train the classification subnet branch with our proposed loss defined in §3.2. Similar to [26], to address the imbalance between hard and easy examples, we normalize the total classification loss (calculated from $\sim 100k$ anchors) by the total number of object/positive anchor boxes rather than the total number of anchors. We use standard smooth L_1 loss for the box-regression subnet branch. The total training loss is the sum of the loss of both branches.

Inference: For seen object detection, a simple forward pass predicts both confidence scores and bounding boxes in the classification and box-regression subnetworks respectively. Note that we only consider a fixed number (e.g., 100) of boxes from RPN having confidence greater than 0.05 for inference. Moreover, we apply Non-Maximum Suppression (NMS) with a threshold of 0.5 to obtain final detections. We select the final detections that satisfy a seen score-threshold (t_s). To detect unseen objects, we use the following equation, followed by an unseen score-thresholding with a relatively lower value ($t_u < t_s$)²:

$$\mathbf{p}_u = W_u W_s^T \sigma(\delta(W_s M D) \mathbf{f}) \quad (9)$$

where, $W_u \in \mathbb{R}^{U \times d}$ contains unseen class word vectors. For generalized zero-shot object detection (GZSD), we simply consider all detected seen and unseen objects together. In our experiments, we report performances for traditional seen, zero-shot unseen detection and GZSD. One can notice that our architecture predicts a bounding box for every anchor which is independent of seen classes. It enables the network to predict bounding boxes dedicated to unseen objects. The previous attempt like [36] detects seen objects first and then attempts to classify those detections to unseen objects based on semantic similarity. By contrast, our model allows detection of unseen bounding boxes that are different to those seen.

²Our experiments show that threshold values $t_s = 0.3$ and $t_u = 0.1$ generally work well. Note that t_u is kept smaller to counter classifier bias towards unseen classes due to the lack of visual examples during training.

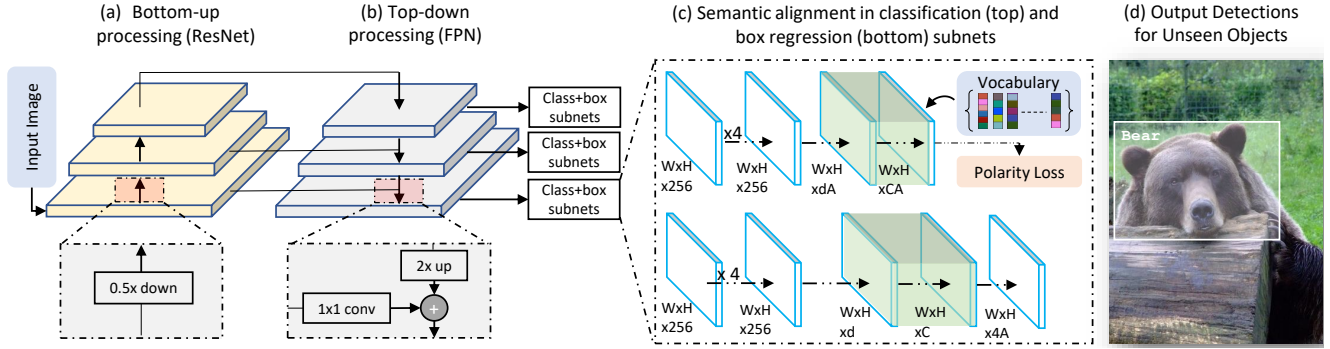


Figure 5: Network architecture for ZSD. The green colored layer implements Eq. 7 (Our-word) or 8 (Our-vocab).

Reduced description of unseen: As proposed in [35], all the seen semantics vectors may not necessary to describe an unseen object. Thus, we only consider top T predictions, $\mathbf{p}'_v \in \mathbb{R}^T$ from $\sigma(\delta(W_sMD)\mathbf{f})$ and the corresponding seen word vectors, $W'_s \in \mathbb{R}^{T \times d}$ to predict unseen scores. For the reduced case, $\mathbf{p}'_u = W_u W'_s \mathbf{p}'_v$. In the experiment, we vary the number of the closest seen T from 5 to S and find that a relatively small value of T (e.g., 5) performs better than using all available $T = S$ seen word vectors.

6. Experiments

6.1. Setup

Datasets: We evaluated our approach with two different settings of MS-COCO (2014) [28] and a single setting of Pascal VOC (2007/12) [9]. With 80 object classes, MS-COCO includes 82,783 training and 40,504 validation images. In a typical ZSD setting, only unseen class performance is of interest. As the test data labels are not known, the ZSD evaluation is done on a subset of validation data. MS-COCO (2014) has more validation images than any later versions which motivates us to use the 2014 version. For Pascal VOC, we use the train set of 2007 and 2012 for training and use validation+test set of 2007 for testing.

Issues with existing MS-COCO split: Recently, [5] proposed a split of seen/unseen classes for MS-COCO (2014). It considers 73,774 training images from 48 seen classes and 6608 test images from 17 unseen classes. The split criteria were the cluster embedding of class word-vectors in the semantic space and synset WordNet hierarchy [31]. We identify two practical drawbacks of this split: (1) Because all 63 classes are not used as seen, this split does not take full advantage of training images/annotations, (2) Because of choosing unseen classes based on wordvector clustering it cannot guarantee the desired diverse nature of the unseen set. For example, this split does not choose any classes from ‘outdoor’ super-category of MS-COCO.

Proposed seen/unseen split on MS-COCO: To address these issues, we propose a more realistic split of MS-COCO

for ZSD. Following the practical consideration of unseen classes discussed in [36] i.e. rarity and diverseness, we follow the following steps to create split: (1) We sort classes of each superclass in ascending order based on the total number of instances in the training set. (2) For each superclass, we pick 20% rare classes as unseen which results in 15 unseen and 65 seen classes. Note that the superclass information is only used to create a diverse seen/unseen split, and never used during training. (3) Being zero-shot, we remove all the images from the training set where at least one unseen class appears to create a training set of 62,300 images. (4) For testing ZSD, we select 10,098 images from the validation set where at least one instance of an unseen class is present. The total number of unseen bounding boxes is 16,388. We use both seen and unseen annotation together for this set to perform GZSD. (5) We prepare another list of 38,096 images from the validation set where at least one occurrence of the seen instance is present to test traditional detection performance on seen classes. In this paper, we report results on both our and Bansal *et al.* [5] setting.

Pascal VOC Split: For Pascal VOC 2007/12 [9], we follow the split proposed in [8]. We use 16 seen and 4 unseen classes from total 20 classes. We utilize 2072 and 3909 train images from Pascal VOC 2007 and 2012 respectively after ignoring images containing any instance of unseen classes. For testing, we use 1402 val+test images from Pascal VOC 2007 where any unseen class appears at least once.

Vocabulary: We choose vocabulary atoms from 5018 Flickr tags in NUS-WIDE [7]. From this list, we only remove MS-COCO class names and tags which have no word vectors. This vocabulary covers a wide variety of objects, attributes, scene types, actions, and visual concepts.

Semantic embedding: For MS-COCO classes and vocabulary words of NUS-WIDE [7], we use ℓ_2 normalized 300 dimensional unsupervised word2vec [30], GloVe [33] and FastText [17] vectors obtained from billions of words from unannotated texts like Wikipedia. As suggested by [8], for Pascal VOC [9] classes, we use average 64 dimension binary per-instance attribute annotation of all training

Method	Seen / Unseen	ZSD (mAP/RE)	Seen (mAP/RE)	Unseen (mAP/RE)	HM (mAP/RE)
Split in [5] (\downarrow)					
Bansal <i>et al.</i> [5]	48/17	0.70/27.19	-/15.02	-/15.32	-/15.17
FL-word	48/17	5.91/18.67	36.57/42.21	2.64/17.60	4.93/24.84
Our-word	48/17	6.99/19.54	35.40/39.02	3.18/18.85	5.84/25.42
Our-vocab	48/17	10.01/43.56	35.92/38.24	4.12/26.32	7.39/31.18
Proposed Split (\downarrow)		mAP	mAP	mAP	mAP
FL-basic	65/15	8.68	38.29	8.68	14.15
FL-word	65/15	10.80	37.56	10.80	16.77
FL-vocab	65/15	12.04	37.31	12.05	18.22
Our-word	65/15	12.02	33.28	12.02	17.66
Our-vocab	65/15	12.62	32.99	12.62	18.26



Figure 6: (left) Overall performance on MS-COCO. $\beta=20$, IoU=0.5, Recall@100. mAP = mean average precision and RE = recall. The top part shows results on Bansal *et al.* [5] split and the lower part shows results on our proposed split. Our-vocab achieves best performance in terms of mAP on unseen classes. (Right) Qualitative examples of ZSD (top row) and GZSD (bottom row). Pink and yellow box represent unseen and seen detections respectively. See supplementary material for more qualitative results.

γ	α	FL-vocab (mAP)			Our-vocab (mAP)		
		ZSD	GZSD		ZSD	GZSD	
			Seen	Unseen		Seen	Unseen
0	1	0	0	0	6.6	31.9	6.6
0	.75	2.4	11.9	2.3	3.9	2.7	27.4
0.1	.75	4.0	12.3	4.0	6.0	5.4	27.9
0.2	.75	6.2	27.8	6.2	10.1	7.3	31.4
0.5	.50	7.0	31.2	7.0	11.5	8.4	30.6
1.0	.25	10.8	35.8	10.8	16.6	11.6	31.3
2.0	.25	12.0	37.3	12.1	18.2	12.6	33.0
5.0	.25	8.7	37.2	8.7	14.2	9.1	33.6

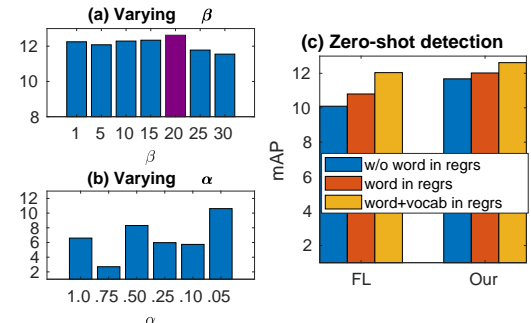


Figure 7: Ablation studies: (Left) Sensitivity Analysis: varying α and γ with a fixed $\beta=20$. (Right-a) Impact of varying β , (Right-b) varying α with $\gamma=0$ to see the behavior of our loss with only balanced CE. (Right-c) Impact of word-vectors in the regression branch.

images from aPY dataset [10]. Unless mentioned otherwise, we use word2vec while reporting performance in this paper. See supplementary material for experimental details.

6.2. Quantitative Results

Compared Methods: We rigorously evaluate our proposed ZSD method on both Bansal *et al.*’s split [5] (48/17) and our new (65/15) split of MS-COCO. We provide a brief description of all compared methods: **(a)** Bansal *et al.* [5]: This method extracts pre-trained Inception-ResNet-v2 features from Edge-Box object proposals. It applies a standard max-margin loss to align visual features to semantic embeddings via linear projections. As [5] reported recall performances, we also report recall results (in addition to mAP) to compare with this method. **(b)** FL-basic: This method trains an exact RetinaNet model. Thus, it does not use any word vectors during training. To extend this approach to perform ZSD, we apply this formula to calculate unseen scores: $\mathbf{p}'_u = W_u W_s^{T} \mathbf{p}'_d$ where \mathbf{p}'_d represents top T seen prediction scores for the reduced description of unseen. **(c)** FL-word: This method is based on the architecture in Fig. 3(b). It uses static word vectors during training. But, it can-

not update the vectors based on visual features. It uses focal loss for training. **(d)** Our-word: Exact same architecture of FL-word but training is done with our proposed polarity loss. **(e)** FL-vocab: The method uses our proposed framework in Fig. 5 with vocabulary metric learning in the custom layer but operates on focal loss. **(f)** Our-vocab: This method is our final proposal using vocabulary metric learning and proposed polarity loss (Fig. 5).

Overall Results: Fig. 6 presents overall performance on ZSD and GZSD tasks across different comparison methods with two different seen/unseen split settings of MS-COCO. In addition to mAP, we also report recall (RE) to compare with [5]. We observe the following trends in our results: **(1)** With 48/17 settings, our method beats [5] in both the ZSD and GZSD tasks by a significantly large margin. This improvement is the result of end-to-end learning, the inclusion of the vocabulary metric to update word vectors and the proposed loss in our method. **(2)** With 65/15 settings, FL-word works better than FL-basic for ZSD and GZSD because the former uses seen word vectors during training whereas the later does not adopt semantics. By contrast, in GZSD-seen detection cases, FL-basic out-



Method	Overall	airplane	train	parking meter	cat	bear	suitcase	frisbee	snowboard	fork	sandwich	hot dog	toilet	mouse	toaster	hair drier
FL-vocab	12.0	13.4	41.8	0.6	34.8	18.7	12.6	19.4	16.9	8.9	8.7	1.0	3.7	.04	0.2	.03
Our-vocab	12.6	22.9	48.0	0.6	24.0	12.5	12.9	27.9	14.8	8.3	7.5	1.2	8.4	0.1	0.2	.02

Table 2: Per-class AP of MS-COCO unseen classes using our proposed split. Our-vocab achieves better performance in more unseen classes than FL-vocab.

Method	Seen	Unseen	aeroplane	bicycle	bird	boat	bottle	bus	cat	chair	cow	d.table	horse	motorbike	person	pplant	sheep	tvmonitor	car	dog	sofa	train
[8]	57.9	54.5	68.0	72.0	74.0	48.0	41.0	61.0	48.0	25.0	48.0	73.0	75.0	71.0	73.0	33.0	59.0	57.0	55.0	82.0	55.0	26.0
Our	63.5	62.1	74.4	71.2	67.0	50.1	50.8	67.6	84.7	44.8	68.6	39.6	74.9	76.0	79.5	39.6	61.6	66.1	63.7	87.2	53.2	44.1

Table 3: mAP values for Pascal VOC’07 classes. *Italic* classes are unseen.

performs FL-word because the use of unsupervised semantics (word vectors) during training in FL-word introduces noise in the network which degrades the seen performance. (3) Again, from FL-word to FL-vocab unseen performances improve. The use of the vocabulary metric in FL-vocab helps the word vectors to update based on visual similarity which allows visual features to align better with their semantics. (4) Our-vocab further improves the ZSD performance because of the proposed loss which increases inter-class and reduces intra-class differences. It brings better alignment among visual and semantic subspaces than FL. We report more results on GloVe and FastText word vectors in the supplementary material.

Hyper-parameter Sensitivity Analysis: Here, we show the effect of loss hyper-parameters γ , α and β . First, we vary $\gamma \in [0, 5]$ and $\alpha \in [.25, 1]$ keeping $\beta=20$. As α and β are originally FL parameters, we choose the values used in [26]. In Fig. 7 (left), we report mAP of FL-vocab and Our-vocab methods using these parameter settings for ZSD and GZSD tasks. We notice that with a fixed $\beta=20$ for Our-vocab consistently outperforms FL-vocab. This shows that our loss helps in improving ZSD and GZSD performance. We also vary β from 1-30 to see its effect on ZSD in Fig. 7 (Right-a). This parameter controls the steepness of the penalty function f_p in Eq. 5. For poorly classified cases, when $p^i - p^l \approx 0$, the penalty function calculates the appropriate loss. We notice that $\beta = 20$ provides correct steepness to calculate a penalty for incorrect predictions. Our loss can also work reasonably well with only balanced CE (i.e., without FL when $\gamma=0$). We illustrate this in Fig. 7 (Right-b). With a low α of 0.05, our method can achieve around 10% mAP. It shows that our penalty function can effectively balance object/background and easy/hard examples. More ablation studies on the reduced description of unseen and IoU are included in the supplementary material.

Semantics in box-regression subnet: Our framework can be trained without semantics in the box-regression subnet. In Fig. 7 (Right-c), we compare performances with and without using word vectors in the regression branch using

FL and our loss. We observe that using word vectors in regression branch helps to improve the performance of ZSD.

Individual class results: We present per class results on MS-COCO (with our proposed split) and Pascal VOC 2007 (with Demirel *et al.*’s [8] split) in Table 2 and 3 respectively. Considering the complexity of the MS-COCO dataset, we achieve decent performance (above 10 mAP) in airplane, train, cat, bear, suitcase, frisbee and snowboard. Our model performs poorly (below 10 mAP) on parking meter, fork, sandwich, hot dog, toilet, mouse, toaster, and hair drier because there are fewer similar visual instances in training and a lack of similar seen classes. To compare with YOLO-based ZSD [8], we adopt their exact settings with Pascal VOC 2007 and 2012. Note that, their approach used attribute vectors as semantics from [10]. As such attribute vectors are not available for our vocabulary list, we compare this approach with only using fixed attribute vectors inside our network. Our method outperforms [8] by a large margin (57.9 vs 63.5 on traditional seen detection, 54.5 vs 62.1 on unseen detection). The proposed loss helps our method to achieve this improvement.

7. Conclusion

In this paper, we attempt a sophisticated version of the zero-shot learning task, zero-shot object detection (ZSD). We propose an end-to-end trainable framework of ZSD which includes a novel loss formulation and facility to update semantic domain based on the visual-word relation. Our proposed loss penalizes an example considering background vs. object imbalance, easy vs. hard difference and inter-class vs. intra-class relations. Moreover, our approach learns a vocabulary metric to reshape the semantic embedding space so that word-vectors become well-distributed and visually similar classes reside close together inside the embedding. Also, we propose a realistic seen-unseen split on the MS-COCO dataset to evaluate ZSD methods. In our experiments, we have outperformed several recent state-of-the-art methods on both ZSD and GZSD tasks across the MS-COCO and Pascal VOC 2007 datasets.

References

- [1] Z. Al-Halah and R. Stiefelhagen. Automatic discovery, association estimation and learning of semantic attributes for a thousand categories. In *The IEEE Conference on Computer Vision and Pattern Recognition (CVPR)*, 2017. [5](#), [11](#)
- [2] Z. Al-Halah, M. Tapaswi, and R. Stiefelhagen. Recovering the missing link: Predicting class-attribute associations for unsupervised zero-shot learning. In *The IEEE Conference on Computer Vision and Pattern Recognition (CVPR)*, June 2016. [5](#), [11](#)
- [3] A. J. Anderson, E. Bruni, A. Lopopolo, M. Poesio, and M. Baroni. Reading visually embodied meaning from the brain: Visually grounded computational models decode visual-object mental imagery induced by written text. *NeuroImage*, 120:309–322, 2015. [2](#)
- [4] A. J. Anderson, D. Kiela, S. Clark, and M. Poesio. Visually grounded and textual semantic models differentially decode brain activity associated with concrete and abstract nouns. *Transactions of the Association of Computational Linguistics*, 5(1):17–30, 2017. [2](#)
- [5] A. Bansal, K. Sikka, G. Sharma, R. Chellappa, and A. Divakaran. Zero-shot object detection. In *The European Conference on Computer Vision (ECCV)*, September 2018. [1](#), [2](#), [4](#), [6](#), [7](#), [12](#)
- [6] M. Bojarski, D. Del Testa, D. Dworakowski, B. Firner, B. Flepp, P. Goyal, L. D. Jackel, M. Monfort, U. Muller, J. Zhang, et al. End to end learning for self-driving cars. *arXiv preprint arXiv:1604.07316*, 2016. [13](#)
- [7] T.-S. Chua, J. Tang, R. Hong, H. Li, Z. Luo, and Y.-T. Zheng. Nus-wide: A real-world web image database from national university of singapore. In *CIVR*, Santorini, Greece., July 8-10, 2009. [6](#)
- [8] B. Demirel, R. G. Cinbis, and N. Ikizler-Cinbis. Zero-shot object detection by hybrid region embedding. In *British Machine Vision Conference (BMVC)*, Sep. 2018. [1](#), [2](#), [6](#), [8](#), [12](#)
- [9] M. Everingham, L. Van Gool, C. K. Williams, J. Winn, and A. Zisserman. The pascal visual object classes (voc) challenge. *International journal of computer vision*, 88(2):303–338, 2010. [6](#)
- [10] A. Farhadi, I. Endres, D. Hoiem, and D. Forsyth. Describing objects by their attributes. In *CVPR*, pages 1778–1785. IEEE, 2009. [7](#), [8](#)
- [11] R. Felix, V. B. G. Kumar, I. Reid, and G. Carneiro. Multi-modal cycle-consistent generalized zero-shot learning. In *The European Conference on Computer Vision (ECCV)*, September 2018. [11](#)
- [12] Y. Fu, T. Xiang, Y. Jiang, X. Xue, L. Sigal, and S. Gong. Recent advances in zero-shot recognition: Toward data-efficient understanding of visual content. *IEEE Signal Processing Magazine*, 35(1):112–125, Jan 2018. [2](#)
- [13] K. He, X. Zhang, S. Ren, and J. Sun. Deep residual learning for image recognition. volume 2016-January, pages 770–778, 2016. cited By 107. [2](#), [5](#), [12](#)
- [14] R. Hu, H. Xu, M. Rohrbach, J. Feng, K. Saenko, and T. Darrell. Natural language object retrieval. In *CVPR*, pages 4555–4564, 2016. [2](#)
- [15] S. Jetley, M. Sapienza, S. Golodetz, and P. H. Torr. Straight to shapes: Real-time detection of encoded shapes. *arXiv preprint arXiv:1611.07932*, 2016. [2](#)
- [16] K. H. J. S. Jifeng Dai, Yi Li. R-FCN: Object detection via region-based fully convolutional networks. *arXiv preprint arXiv:1605.06409*, 2016. [2](#)
- [17] A. Joulin, E. Grave, P. Bojanowski, and T. Mikolov. Bag of tricks for efficient text classification. volume 2, pages 427–431, 2017. [6](#), [13](#)
- [18] E. Kodirov, T. Xiang, Z. Fu, and S. Gong. Unsupervised domain adaptation for zero-shot learning. In *The IEEE International Conference on Computer Vision (ICCV)*, December 2015. [11](#)
- [19] E. Kodirov, T. Xiang, and S. Gong. Semantic autoencoder for zero-shot learning. In *CVPR*, July 2017. [2](#), [11](#)
- [20] T. Kong, F. Sun, C. Tan, H. Liu, and W. Huang. Deep feature pyramid reconfiguration for object detection. In *The European Conference on Computer Vision (ECCV)*, September 2018. [2](#)
- [21] C. H. Lampert, H. Nickisch, and S. Harmeling. Attribute-based classification for zero-shot visual object categorization. *IEEE Transactions on Pattern Analysis and Machine Intelligence*, 36(3):453–465, March 2014. [2](#), [11](#)
- [22] C.-W. Lee, W. Fang, C.-K. Yeh, and Y.-C. Frank Wang. Multi-label zero-shot learning with structured knowledge graphs. In *The IEEE Conference on Computer Vision and Pattern Recognition (CVPR)*, June 2018. [2](#)
- [23] Z. Li, E. Gavves, T. Mensink, and C. G. Snoek. Attributes make sense on segmented objects. In *European Conference on Computer Vision*, pages 350–365. Springer, 2014. [2](#)
- [24] Z. Li, C. Peng, G. Yu, X. Zhang, Y. Deng, and J. Sun. Detnet: Design backbone for object detection. In *The European Conference on Computer Vision (ECCV)*, September 2018. [2](#)
- [25] Z. Li, R. Tao, E. Gavves, C. Snoek, and A. Smeulders. Tracking by natural language specification. In *CVPR*, pages 6495–6503, 2017. [2](#)
- [26] T. Lin, P. Goyal, R. Girshick, K. He, and P. Dollar. Focal loss for dense object detection. *IEEE Transactions on Pattern Analysis and Machine Intelligence*, pages 1–1, 2018. [2](#), [5](#), [8](#), [12](#)
- [27] T.-Y. Lin, P. Dollar, R. Girshick, K. He, B. Hariharan, and S. Belongie. Feature pyramid networks for object detection. In *The IEEE Conference on Computer Vision and Pattern Recognition (CVPR)*, July 2017. [2](#), [12](#)
- [28] T.-Y. Lin, M. Maire, S. Belongie, J. Hays, P. Perona, D. Ramanan, P. Dollár, and C. L. Zitnick. Microsoft coco: Common objects in context. In *ECCV*, pages 740–755. Springer, 2014. [6](#)
- [29] W. Liu, D. Anguelov, D. Erhan, C. Szegedy, S. Reed, C.-Y. Fu, and A. C. Berg. *SSD: Single Shot MultiBox Detector*, pages 21–37. Springer International Publishing, Cham, 2016. [2](#)
- [30] T. Mikolov, I. Sutskever, K. Chen, G. S. Corrado, and J. Dean. Distributed representations of words and phrases and their compositionality. In C. J. C. Burges, L. Bottou, M. Welling, Z. Ghahramani, and K. Q. Weinberger, editors, *NIPS*, pages 3111–3119. Curran Associates, Inc., 2013. [6](#), [11](#)

[31] G. A. Miller. Wordnet: a lexical database for english. *Communications of the ACM*, 38(11):39–41, 1995. 6

[32] A. Paivio. Dual coding theory: Retrospect and current status. *Canadian Journal of Psychology/Revue canadienne de psychologie*, 45(3):255, 1991. 1

[33] J. Pennington, R. Socher, and C. D. Manning. Glove: Global vectors for word representation. In *EMNLP*, pages 1532–1543, 2014. 6, 11, 13

[34] S. Rahman and S. Khan. Deep multiple instance learning for zero-shot image tagging. In *Asian Conference on Computer Vision (ACCV)*, December 2018. 2

[35] S. Rahman, S. Khan, and F. Porikli. A unified approach for conventional zero-shot, generalized zero-shot, and few-shot learning. *IEEE Transactions on Image Processing*, 27(11):5652–5667, Nov 2018. 2, 6, 11

[36] S. Rahman, S. Khan, and F. Porikli. Zero-shot object detection: Learning to simultaneously recognize and localize novel concepts. In *Asian Conference on Computer Vision (ACCV)*, December 2018. 1, 2, 5, 6

[37] J. Redmon and A. Farhadi. Yolo9000: Better, faster, stronger. In *The IEEE Conference on Computer Vision and Pattern Recognition (CVPR)*, July 2017. 2

[38] S. Ren, K. He, R. Girshick, and J. Sun. Faster r-cnn: Towards real-time object detection with region proposal networks. *IEEE Transactions on Pattern Analysis and Machine Intelligence*, 39(6):1137–1149, June 2017. 2

[39] Z. Ren, H. Jin, Z. Lin, C. Fang, and A. Yuille. Multiple instance visual-semantic embedding. In *BMVC*, 2017. 2

[40] J. Schmidhuber. Deep learning in neural networks: An overview. *Neural networks*, 61:85–117, 2015. 13

[41] K. Simonyan and A. Zisserman. Very deep convolutional networks for large-scale image recognition. *arXiv preprint arXiv:1409.1556*, 2014. 2

[42] J. Song, C. Shen, Y. Yang, Y. Liu, and M. Song. Transductive unbiased embedding for zero-shot learning. In *The IEEE Conference on Computer Vision and Pattern Recognition (CVPR)*, June 2018. 11

[43] L. Van Der Maaten. Accelerating t-sne using tree-based algorithms. *Journal of machine learning research*, 15(1):3221–3245, 2014. 5

[44] Y. Xian, Z. Akata, G. Sharma, Q. Nguyen, M. Hein, and B. Schiele. Latent embeddings for zero-shot classification. In *The IEEE Conference on Computer Vision and Pattern Recognition (CVPR)*, June 2016. 11

[45] Y. Xian, C. H. Lampert, B. Schiele, and Z. Akata. Zero-shot learning - a comprehensive evaluation of the good, the bad and the ugly. *IEEE Transactions on Pattern Analysis and Machine Intelligence*, pages 1–1, 2018. 2, 12

[46] H. Xu, X. Lv, X. Wang, Z. Ren, N. Bodla, and R. Chellappa. Deep regionlets for object detection. In *The European Conference on Computer Vision (ECCV)*, September 2018. 2

[47] Y. Yu, Z. Ji, J. Guo, and Z. Zhang. Zero-shot learning via latent space encoding. *IEEE transactions on cybernetics*, (99):1–12, 2018. 11

[48] Y. Yu, Z. Ji, X. Li, J. Guo, Z. Zhang, H. Ling, and F. Wu. Transductive zero-shot learning with a self-training dictionary approach. *IEEE Transactions on Cybernetics*, 48(10):2908–2919, Oct 2018. 11

[49] L. Zhang, T. Xiang, and S. Gong. Learning a deep embedding model for zero-shot learning. In *CVPR*, July 2017. 2, 11

[50] A. Zhao, M. Ding, J. Guan, Z. Lu, T. Xiang, and J.-R. Wen. Domain-invariant projection learning for zero-shot recognition. 11

[51] P. Zhu, H. Wang, T. Bolukbasi, and V. Saligrama. Zero-shot detection. *arXiv preprint arXiv:1803.07113*, 2018. 1, 2, 4

[52] C. L. Zitnick and P. Dollár. Edge boxes: Locating object proposals from edges. In D. Fleet, T. Pajdla, B. Schiele, and T. Tuytelaars, editors, *ECCV*, pages 391–405, Cham, 2014. Springer International Publishing. 2

Supplementary Material for “Polarity Loss for Zero-shot Object Detection”

Shafin Rahman^{*†}, Salman Khan^{†‡*} and Nick Barnes^{†*}

^{*}Australian National University, [†]Data61-CSIRO, [‡]Inception Institute of AI

firstname.lastname@anu.edu.au

Abstract

This Supplementary Material provides additional details in support of the discussion presented in the main paper.

- *Section 8: Related work on Zero-shot learning (ZSL) (additional discussion in support of Section 2 of the main paper)*
- *Section 9: Alternative formulation of Polarity loss (additional discussion in support of Section 3.2 of the main paper)*
- *Section 10: Architecture details (additional discussion in support of Section 5 of the main paper)*
- *Section 11: Experimental details (additional discussion in support of Section 6.1 of the main paper)*
- *Section 12: More results (additional discussion in support of Section 6.2 of the main paper)*

8. Related work on Zero-shot learning (ZSL)

The earliest efforts were based on manually annotated attributes as a mid-level semantic representation [21]. This approach resulted in a decent performance on fine-grained recognition tasks but to eliminate strong attribute supervision; researchers start exploring unsupervised word-vector [30, 33] based techniques. Independent of the source of semantic information, a typical ZSL method needs to map both visual and semantic features to a common space to properly align information available in both domains. This can be achieved in three ways: (a) transform the image feature to semantic feature space [35], (b) map the semantic feature to image feature space [49, 19] or, (c) map both image or semantic features to a common intermediate latent space [44, 47]. To apply ZSL in practice, few notable problem settings are: (1) transductive ZSL [42, 48]: making use of unlabeled unseen data during training, (2) generalized ZSL [11, 35]: classifying seen and unseen classes together,

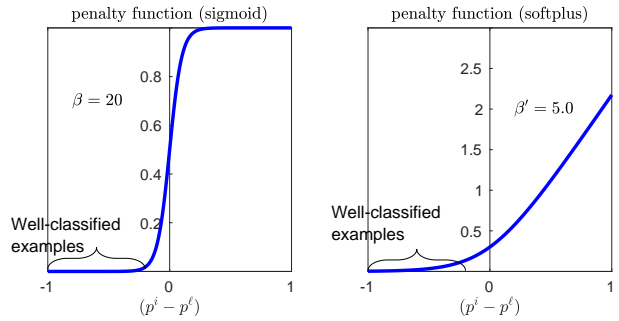


Figure 8: Visualization of sigmoid (left) vs. softplus (right) based penalty function.

(3) domain adaptation [18, 50]: learning a projection function to adapt unseen target to seen source domain, (4) class-attribute association [2, 1]: relating unsupervised semantics to human recognizable attributes. In this paper, our focus is not only the recognition but also simultaneous localization of unseen objects which is a significantly complex and challenging problem.

9. Alternative formulation of polarity loss

We have used a sigmoid based penalty function to implement $f_p(p^i - p^\ell)$ in our proposed polarity loss. Now, we present an alternative implementation of the penalty function based on softplus function. In Fig. 8, we illustrate the shapes of both sigmoid and softplus based penalty functions. Both the functions increase penalty when $p^i - p^\ell$ moves from -1 to 1 . However, softplus is relatively smoother than sigmoid. Also, softplus has a flexibility to assign a penalty > 1 for any poorly classified examples whereas sigmoid can penalize at most 1. The formulation for softplus based penalty function is as follows,

$$f_p(p^i - p^\ell) = \log(1 + e^{\beta'(p^i - p^\ell)}) \quad (10)$$

Method	Penalty Function	Seen/Unseen	Word Vector	ZSD (mAP)	GZSD		
					seen (mAP)	unseen (mAP)	HM (mAP)
Our-vocab	softplus	65/15	w2v	12.17	32.12	12.18	17.66
Our-vocab	sigmoid	65/15	w2v	12.62	32.99	12.62	18.26

Table 4: Comparison of ZSD performance with softplus and sigmoid based penalty functions.

where, β' is the loss hyper-parameter. The final polarity loss with softplus based penalty function is the following:

$$\mathcal{L}_{PL}(\mathbf{p}, \mathbf{y}) = \sum_i -\alpha_t^i (1 - p_t^i)^\gamma \log \left(1 + e^{\beta'(p^i - p^\ell)} \right) \log p_t^i,$$

$$p_t^i = \begin{cases} p^i, & \text{if } y^i = 1 \\ 1 - p^i, & \text{otherwise} \end{cases} \quad p^\ell = p^i \llbracket y^i = 1 \rrbracket, \quad (11)$$

where $\llbracket \cdot \rrbracket$ denotes the Iverson bracket.

In the first row of Table 4, we report performance of Our-vocab using this alternative polarity loss with $\beta' = 5$ and word2vec as semantic information. With this alternative formulation, we achieve a performance quite close to that of sigmoid based polarity loss.

10. Architecture details

Our network architecture is based on the RetinaNet model [26]. RetinaNet has one backbone network called Feature Pyramid Network (FPN) [27] and two task-specific subnetwork branches for classification and box regression. FPN extracts rich, multi-scale features for different anchor boxes from an image to detect objects at different scales. For each pyramid level, we use anchors at $\{1:2, 1:1, 2:1\}$ aspect ratios with sizes $\{2^0, 2^{1/3}, 2^{2/3}\}$ totaling to $A=9$ anchors per level, covering an area of 32^2 to 512^2 pixels. The classification and box-regression subnetworks attempt to predict the one-hot target ground-truth vector of size S and box parameters of size four respectively. We consider an anchor box as an object if it gets an intersection-over-union (IoU) ratio > 0.5 with a ground-truth bounding box.

Modifications to RetinaNet: Suppose, a feature map at a given pyramid level has C channels. For the **classification subnet**, we first apply four conv layers with C filters of size 3×3 , followed by ReLU, similar to RetinaNet. Afterward, we apply a 3×3 conv layer with $d \times A$ filters to convert visual features to the dimension of word vectors, d . Next, we apply a custom layer which projects image features onto the word vectors. We also apply a sigmoid activation function to the output of the projection. This custom layer may have fixed parameters like Fig. 3(b) or trainable parameters like 3(c) of the main paper with vocabulary metric. These operations are formulated as: $\mathbf{p}_s = \sigma(W_s \mathbf{f})$ or $\mathbf{p}_v = \sigma(\delta(W_s M D) \mathbf{f})$ depending on the implementation of the custom layer. Similarly, for the **box-regression** branch,

we attach another 3×3 convolution layer with C filters and ReLU non-linearity, followed by 3×3 convolution with d filters and the custom layer to get the projection response. Finally, another convolution with $4A$ to predict a relative offset between the anchor and ground-truth box. In this way, the box-prediction branch gets semantic information of word-vectors to predict offsets for regression. Note that, similar to [26], the classification and regression branches do not share any parameters, however, they have a similar structure.

11. Experimental details

Evaluation metric: Being an object detection problem, we evaluate using mean average precision (mAP) at a particular IoU. Unless mentioned otherwise, we use $\text{IoU}=0.5$. Notably, [8] use the Recall measure for evaluations, however since recall based evaluation does not penalize a method for the wrongly predicted bounding boxes, we only recommend mAP based evaluation for ZSD. To evaluate GZSD, we report the harmonic mean (HM) of mAP and recall [5, 45].

MS-COCO split detail: In Fig. 9, we present all 80 MS-COCO classes in a sorted order across each super-category based on the number of instance/bounding boxes inside the training set. Choosing 20% low-instance classes from each super-category ensures the rarity and diverseness for the chosen unseen classes.

Implementation details: We implement FPN with a basic ResNet50 [13]. All images are rescaled to make their smallest side 800px. We train the **FL-basic** method using the original RetinaNet architecture with only training images of seen classes so that the pre-trained network does not get influenced by unseen instances. Then, to train **FL-word**, we use the pre-trained weights to initialize the common layers of our framework. We initialize all other uncommon layers with a uniform random distribution. Similarly, we train **Our-word** and **FL-vocab** upon the training of **FL-word**. Finally, we train **Our-vocab** using the pre-trained network of **FL-vocab**. We train each network for 500k iterations keeping a single image in the minibatch. The only exception while training with our proposed loss is to train for 100k iterations instead of 500k. Each training time varies from 72 to 96 hours using a single Tesla P100 GPU. For optimization, we use Adam optimizer with learn-

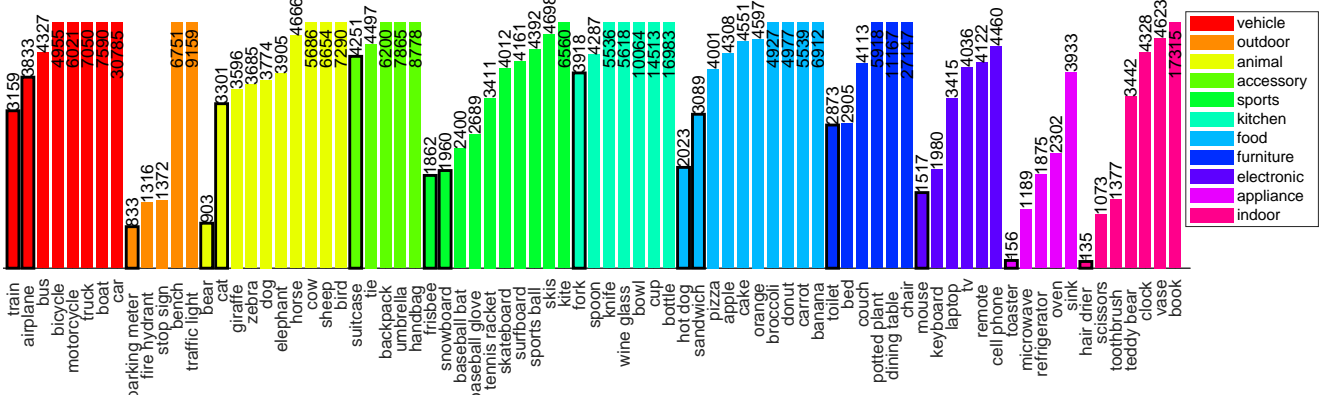


Figure 9: Instances of each class in the MS-COCO dataset (except class ‘person’). Tall bars are clipped for better visualization. The class bars with black border are selected as unseen classes. We choose 20% rarest classes from each superclass as unseen.

ing rate 10^{-5} , $\beta_1 = 0.9$ and $\beta_2 = 0.999$. We implement this framework with *Keras* library.

12. More results

More overall result: In addition to word2vec as semantic word vectors reported in the main paper, we also experiment with GloVe [33] and FastText [17] as word vectors. We report those performances in Table 5. We notice that Glove (glo) and FastText (ftx) achieve respectable performance, although they do not work as well as word2vec. However, in all cases, Our-vocab beats FL-vocab on ZSD in both cases.

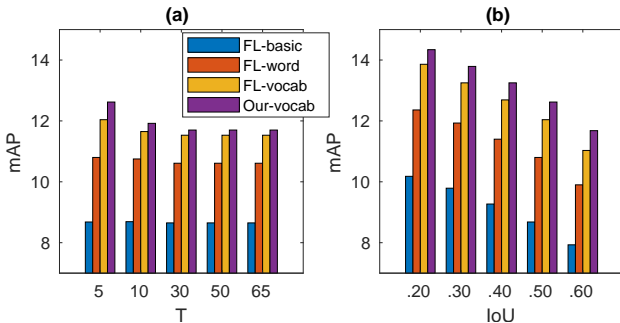


Figure 10: (a) Impact of selecting close seen (b) Impact of IoU.

Varying T and IoU: In Sec. 5 of the main paper, we discussed the reduced description of an unseen class based on closely related seen classes. We experiment with the behavior of our model by varying a different number of close seen classes. One can notice in Fig. 10(a), a smaller number of close seen classes (e.g., 5) results in relatively better performance than using more seen classes (e.g., 10–65) during ZSD prediction. This behavior is related with the average number of classes per superclass (which is 7.2 for MS-COCO excluding ‘person’) because dissimilar classes

from a different superclass may not contribute towards describing a particular unseen class. Thus, we use only five close seen classes to describe an unseen in all our experiments. In Fig. 10(b), we report the impact of choosing a different IoU ratio (from 0.2 to 0.6) in ZSD. As expected, lower IoUs result in better performance than higher ones. As practiced in object detection literature, we use IoU = 0.5 for all other experiments in this paper.

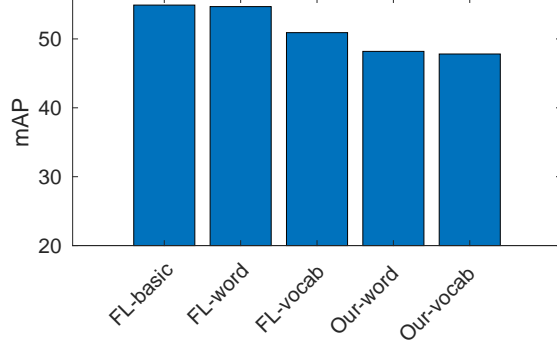


Figure 11: Traditional detection performance on 65 seen classes of MSCOCO.

Traditional detection: We report traditional detection performance of different versions of our framework in Fig. 11. As a general observation, it is clear that making detection explicitly dependent on semantic information hurts the detector’s performance on ‘seen’ classes (traditional detection). This is consistent with the common belief that training directly on the desired output space in an end-to-end supervised setting achieves a better performance [6, 40]. Consistently, we notice that FL-basic achieves the best performance because it is free from the noisy word vectors. FL-word performs relatively worse than FL-basic because of using noise word vectors as class semantics in-

Method	Seen/Unseen	Word Vector	ZSD (mAP)	GZSD		
				seen (mAP)	unseen (mAP)	HM (mAP)
FL-vocab	48/17	ftx	5.68	34.32	2.23	4.19
Our-vocab	48/17	ftx	6.99	35.13	2.73	5.07
FL-vocab	65/15	glo	10.36	36.69	10.33	16.12
Our-vocab	65/15	glo	11.55	36.79	11.53	17.56
FL-vocab	65/15	w2v	12.04	37.31	12.05	18.22
Our-vocab	65/15	w2v	12.62	32.99	12.62	18.26

Table 5: More results on ZSD with different word-vectors (GloVe, FasText and Word2Vec).

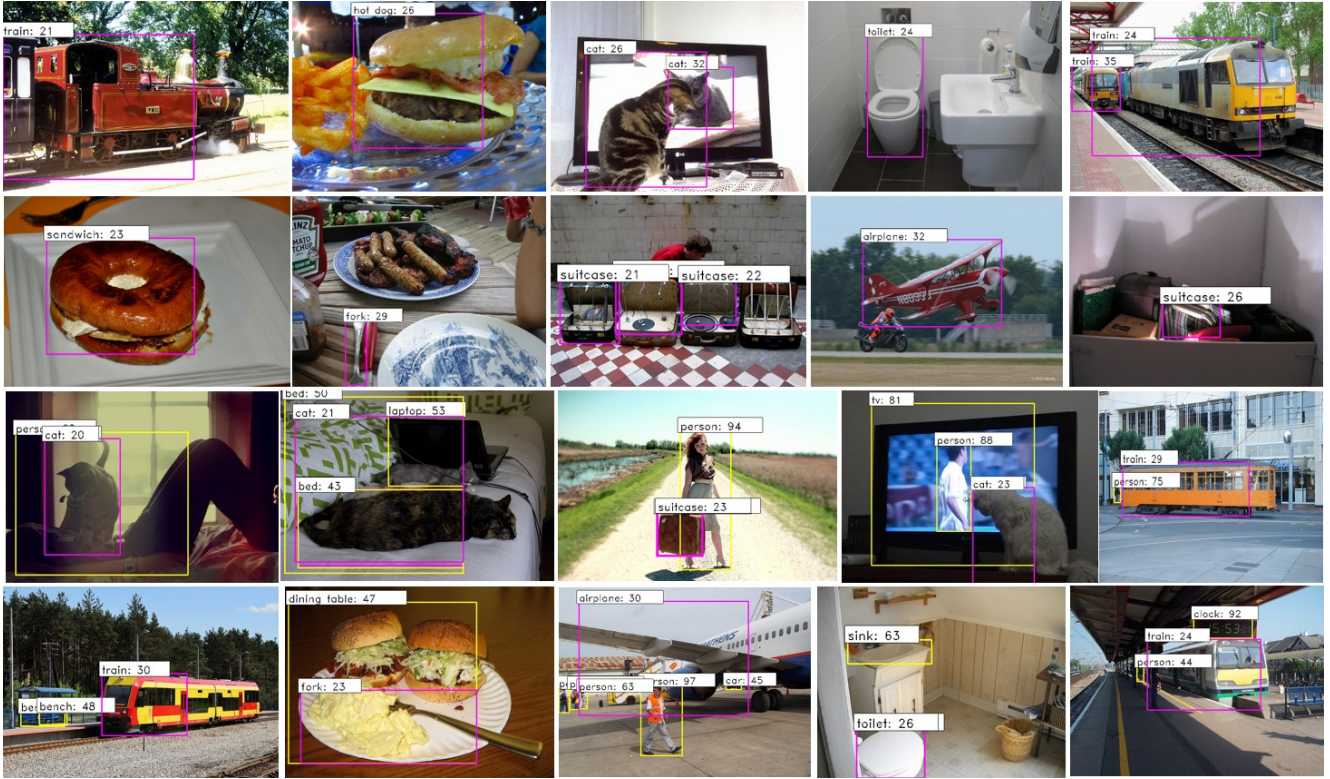


Figure 12: More qualitative results of ZSD (two top rows) and GZSD (two bottom rows). Pink and yellow boxes represent unseen and seen detections respectively.

side the network. Then, word vectors of vocabulary texts further reduce the performance in FL-vocab. Our proposed loss (Our-word and Our-vocab cases) aligns visual features to noisy word vectors better than FL which is valuable for zero-shot learning but slightly degrades the seen performance. Similarly, we notice that while modifying the word embeddings, the vocabulary metric focuses more on proper visual-semantic alignment that is very helpful for ZSD but performs lower for the seen/traditional detection setting.

More qualitative results: In Fig. 12, we show more qualitative results of our approach.